Nanoscale Imaging of the Electronic Conductivity of the Native Oxide Film on Titanium Using Conducting Atomic Force Microscopy

Chett J. Boxley and Henry S. White*

Department of Chemistry, University of Utah, 315 South 1440 East, Salt Lake City, Utah 84112

Catherine E. Gardner and Julie V. Macpherson*

Department of Chemistry, University of Warwick, Coventry CV4 7AL, United Kingdom

Received: April 3, 2003; In Final Form: July 9, 2003

Conducting atomic force microscopy (C-AFM) is used to visualize the heterogeneous electronic conductivity of the native oxide film (nominally a 2.9 nm thick TiO_2 layer) on polycrystalline Ti electrodes (hereafter referred to as Ti/TiO_2 electrodes). Ex situ C-AFM images of Ti/TiO_2 electrodes recorded in air demonstrate that the electronic conductivity of the oxide film in contact with the underlying Ti grain boundaries is at least 200× higher than the conductivity of the oxide film on grain faces. The width of the conductive zone in the oxide film over grain boundaries is estimated to be less than 50 nm (resolution limited by the C-AFM tip size). Small islands of oxide exhibiting high electronic conductivity are also observed on topographically featureless regions of grain faces. The observed spatial variations in conductivity are tentatively attributed to the presence of defects (e.g., Ti^{3+} sites) and lower valence oxides (e.g., Ti_2O_3) in the native oxide film.

Introduction

The stability of many metals in ambient environments results from the presence of a thin surface oxide layer that acts as a kinetic barrier to the transport of ions, molecules, and electrons. For instance, Ti and Al both owe their technological usefulness largely to the spontaneous formation of a 2−3 nm thick surface film of TiO_2 and Al_2O_3, respectively.[1−4] Although the oxide layer on these metals is chemically stable in most oxidizing conditions, recent reports using scanning electrochemical microscopy (SECM) demonstrate that microscopic defect sites within the oxide film can act as efficient shunt pathways for electron transport.[5−9] Localized variations in the thickness, stoichiometry, or crystallography of the oxide film are factors believed to influence the localized conductivity.[5,6]

In the present report, conducting atomic force microscopy (C-AFM) is used to image the heterogeneous electronic conductivity of native oxide films on polycrystalline Ti electrodes with significantly higher resolution than previously possible using SECM. C-AFM has been recently used to investigate the photocatalytic and photoelectrochemical properties of single-crystal TiO_2 (rutile)[10] and nanocrystalline TiO_2 films prepared from a sol−gel.[11] Additional studies have focused on the investigation of the electrical properties of Pt nanoparticles deposited on and in a porous Ti/TiO_2 film.[12] In the current investigation, C-AFM is used to image the conductivity of the native oxide, ex situ, in an attempt to correlate the local electrical properties of the oxide film with previous observations of the local electrochemical activity.[5,6] In the electrochemical measurement, electron transfer between the underlying metal and a soluble redox molecule may occur if the oxide film is sufficiently conductive to allow electron transport, or sufficiently thin to allow direct electron tunneling. The native oxide film on Ti is reported to be 2.9 nm,[1,2] and nominally consists of n-type TiO_2, a large band-gap material ($E_g = 3.05$ eV[13]). An oxide film of this thickness and composition should ideally behave as an insulating film under positive biases, preventing electron transfer between the metal and a solution species. Thus, observations of local electron transfer in electrochemical environments have been previously ascribed to defect structures in the oxide film.

The C-AFM investigation reported herein is the first attempt to directly quantify the heterogeneous electronic defect structure in the native oxide film on Ti. We observe that the conductivity of the oxide film *above grain boundaries* of the underlying polycrystalline Ti electrode is significantly larger than the conductivity of the oxide film on Ti grain faces. Differences in the rate of oxide growth on different crystallographic orientations is well established by optical methods,[14,15] but observations of large variations in conductivity at the intersection of grains has not been reported to the best of our knowledge.

Experimental Section

Chemicals. Water was purified using a Milli-Q (Millipore Corp., Bedford MA) purification system with a resistivity of 18 MΩ cm.

Ti/TiO_2 Electrodes. Ti foil (99.98%, 25 μm thick, Alfa Aesar, Ward Hill MA) was cut into 20 × 20 mm samples. A Cu wire was attached to the corner of each sample using conductive Ag paint (Ag DAG 1415M, Agar Scientific, Essex, U.K.) and insulated using a nonconductive epoxy resin (Araldite, Vantico, Basel Switzerland). Prior to analysis, each sample was first degreased with ethanol, then rinsed thoroughly with water, etched for ∼15 s in a 4% HF and 6% HNO_3 solution,[5] rinsed with copious amounts of water, and dried under a stream of N_2 gas. The Ti/TiO_2 samples were mounted, via double-sided tape, to the AFM sample holder.

Conducting Atomic Force Microscopy. AFM images were recorded using a Digital Instruments Nanoscope E system (DI Inc., Santa Barbara CA) operated in contact mode. Topography images were recorded using both height and deflection modes.

10.1021/jp034874u CCC: $25.00
Published on Web 08/12/2003

In height mode, the changes in the z-piezo position required to maintain a constant cantilever deflection caused by variations in the surface topography, are recorded. In deflection (or error) mode, the signal is a measure of the change in cantilever deflection and is thus the derivative of the height-mode signal. Step edges and other small changes in topography are more distinct in deflection-mode images than in height-mode images.[16] However, quantitative height information on surface structure can only be obtained from height-mode images.

The C-AFM was placed inside a home-built Faraday cage, positioned on a granite benchtop to reduce vibrational noise. Ex situ C-AFM measurements were performed using a waveform generator (Colburn Electronics, Coventry, U.K.) to apply a potential bias between the conducting AFM probe and the substrate. The current was measured using a home-built current amplifier. The set-point force was reduced during imaging to a value just prior to tip disengagement to minimize tip−substrate contact forces and to prevent the tip from inducing current by damaging the oxide layer. Electrical connection to the C-AFM tip was established using the metal spring clasp of the DI fluid cell. The current signal was routed to the input of a signal access module (DI) to acquire the conductivity signal.

As a precaution, either a 1 MΩ resistor (for a +200 mV applied bias) or a 97 MΩ resistor (for a −2.5 mV bias) was inserted in series with the C-AFM tip to prevent damage to the tip or the oxide film resulting from local resistive heating or dielectric breakdown.[17,18,19] Previous scanning tunneling microscopy (STM) studies of Ti/TiO_2 surfaces demonstrate that dielectric breakdown of the native oxide film occurs only when the STM tip is biased to voltages greater than ±0.3 V.[17,20] Luo and co-workers have recently reported irreversible damage to the native Al_2O_3 film on Al during C-AFM imaging at biases above 1.3 V.[19] Our present investigations indicate that μA current levels are acceptable in the C-AFM experiments provided the applied bias voltage remains small, as is the case for the experiments described herein.

The construction of the conductive AFM probes used in these experiments has been described in detail previously.[12,21] The electrical conductivty of each tip was verified before and after each set of experiments by measuring the tip current that flowed when the probe was placed in contact with a metal surface, under an applied bias and in the presence of a current-limiting resistor. In all cases the current response demonstrated no degradation of the tip conductivity between measurements.

Results and Discussion

Local Conductivity of the Native Oxide Film. Figure 1 shows a series of typical deflection and conductivity images of a Ti/TiO_2 sample, obtained simultaneously at progressively higher magnifications (the labels A/A_C, B/B_C, etc, indicate the deflection/conductivity images of the same region, respectively). Absolute values of vertical relief on the order of ~1 μm were estimated from height-mode images (not shown).

The conductivity images in Figure 1, recorded by applying a bias voltage of +200 mV (tip vs substrate), in series with a 1 MΩ resistor, demonstrate that electron conduction across the native oxide film is heterogeneous, with localized regions of high conductivity on length scales ranging from 10^2 to 10^3 nm dispersed within an insulating oxide film. Regions of high conductivity are frequently observed clustered along the edges of the grains of the Ti substrate that are exposed at the surface. This point is clearly illustrated by comparison of images C and C_C in Figure 1, where the deflection image shows an "arrowhead-shaped" grain in the center of the image, and the

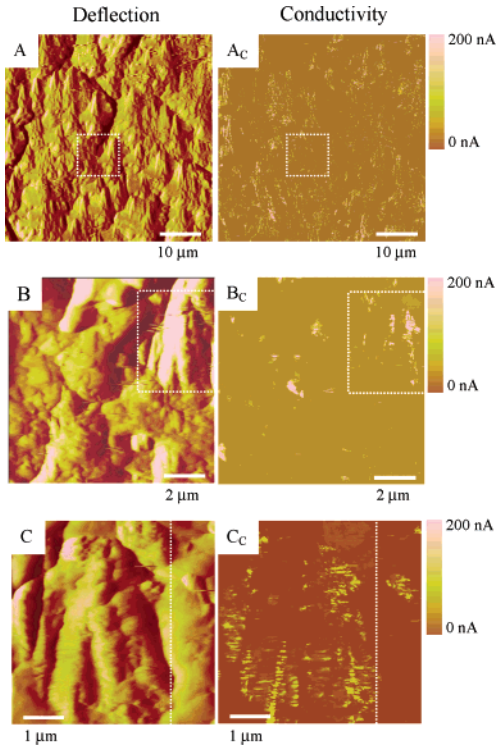

Figure 1. Left-hand column: AFM deflection-mode images of a Ti/TiO_2 surface. Right-hand column: corresponding conductivity images. Images B and B_C and C and C_C correspond to progressively higher magnification of the regions outlined by the boxes (part of images C and C_C to the right of the dotted line are not visible in images B and B_C). $V_B = +200$ mV (tip vs Ti/TiO_2) in series with a 1 MΩ current-limiting resistor.

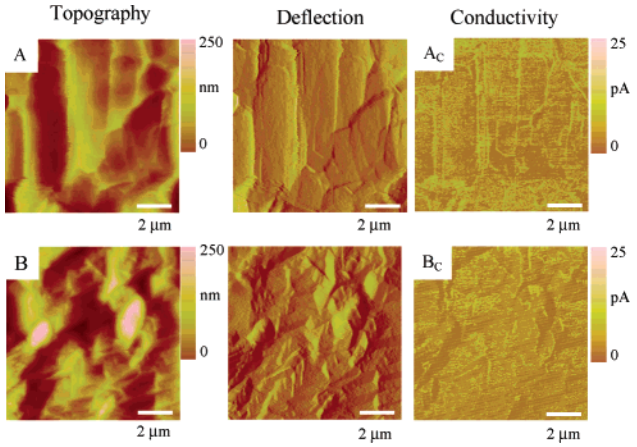

Figure 2. Topography, deflection-mode (images A and B), and conductivity images (A_C and B_C) of two different areas of a Ti/TiO_2 surface. $V_B = -2.5$ mV (tip vs Ti/TiO_2) with a 97 MΩ current-limiting resistor.

corresponding conductivity map shows relatively high conduction along the grain boundary.

Localized conductivity at the grain boundaries is clearer in images where height changes in the substrate topography are less severe, as shown, for example, in Figure 2. Grain boundaries are highlighted in the conductivity images as bright continuous lines of electrical conduction on the surface (images A_C and B_C) and clearly match with grain boundaries in both the height or deflection images (images A and B). The contrast observed in the conductivity images is due to differences in the conductivity of the oxide film, with a higher conductance clearly noticeable over the boundaries between Ti grains. The width of the conductive zones on top of the grain boundary is measured

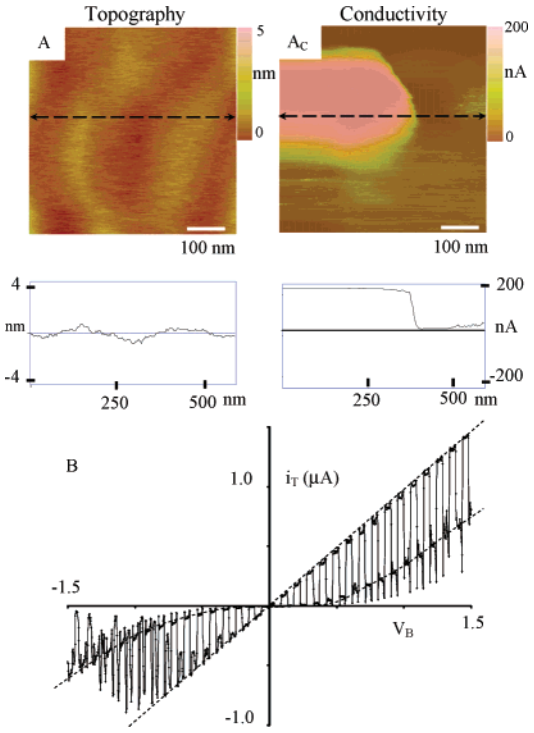

Figure 3. (A) Height-mode topography image (z-scale ~5 nm) and (A_C) conductivity image showing a microscopic area of high conductivity associated with a smooth region of the Ti/TiO_2 surface. Line scans of topography and conductivity are shown directly below the image. (B) Spectroscopic i_T-V_B trace (10 mV s^{-1}) obtained while continuously scanning the C-AFM tip (10 nm s^{-1}) along the dashed line drawn in the conductivity image in (A_C). High and low currents in the i_T-V_B curve correspond to the bright and dark regions, respectively, in the conductivity image.

to be ~50 nm, but this clearly represents an upper limit, as the image resolution is limited by convolution of the tip apex of the C-AFM probe and true feature size.

The shapes and sizes of the grains observed in Figure 2 are entirely consistent with previous transmission electron microscopy (TEM) images of free-standing oxide films, chemically separated and removed from the Ti substrate to yield a replica structure of the underlying Ti grain structure.[9] Both AFM and TEM indicate that the Ti grains are on the order of 1−2 μm in width and 2−4 μm in length.

It is clear that electron transport across the oxide layer is greater above the Ti grain boundaries than across the grain faces. One possibility for this observation is that the oxide layer is significantly thinner over the grain boundary than the average 3 nm thickness reported for the native film, resulting in direct tunneling across the film between the tip and Ti substrate. A more likely possibility is that the oxide layer is highly nonstoichiometric and defective above the grain boundaries, a consequence of the structural mismatch at the intersection between oxide layers growing with different orientation and at different rates on neighboring metal grains.[14,15,22,23] The structure of the oxide layer above the Ti grain boundaries is essentially unknown, but nonstoichiometric structures, e.g., oxygen deficiencies, may result in lower oxides of Ti that are highly conductive.[24−27]

Large fluctuations in oxide film conductivity are observed not only along grain boundaries but also on the grain face. For example, Figure 3 shows a high-resolution C-AFM image of a highly conductive site on the Ti/TiO_2 surface, obtained at a bias voltage of +200 mV. The height-mode image of the region of interest (A) shows that the surface topography is essentially featureless. The corresponding conductivity image (A_C) of the same region, however, reveals a faceted structure that possesses high conductivity. Line scans of the absolute height and conductivity, shown below the corresponding images, demonstrate that a greater than 200-fold increase in conductivity occurs over a ~25 nm wide distance (in this example the current over the conductive feature is limited by a 1 MΩ resistor in series with the tip.) The faceted nature of the highly conductive region clearly suggests that the structure is crystalline. Because very little vertical height variation is observed between this structure and surrounding regions (<1 nm), we speculate that this structure corresponds to a nanocrystallite of a lower valence conducting oxide, e.g., Ti_2O_3.

Ti_2O_3 is a small band-gap semiconductor (E_g ~ 0.1 eV at room temperature) and thus, a nanocrystallite or island of this phase would appear to be highly conductive when embedded in the less conductive TiO_2 phase. Previous Auger and X-ray photoelectron spectroscopic measurements by Armstrong and Quinn[28] of vacuum-deposited Ti clearly demonstrates the presence of the TiO and Ti_2O_3 in the native oxide film. Using electron energy loss and ultraviolet photoemission spectroscopies, Henrich et al.[24] further showed that oxygen vacancies created on the surface of TiO_2 single crystals result in the formation of isolated islands of ordered Ti_2O_3 (albeit the island dimensions were not determined). Thus, although our C-AFM measurements do not provide direct assessment of the chemical identity of the more conductive surface regions, it appears highly likely that these regions correspond to the lower valence oxides previously identified by spectroscopic methods.

The electrical characteristics of the conducting and nonconducting regions in Figure 3 were investigated by recording the tip current (i_T) as a function of the bias voltage (V_B). To obtain the i_T-V_B curve, Figure 3B, the slow scan axis of the C-AFM was disabled such that the tip traced the same line repeatedly at 10 nm s^{-1} (dashed line in images A and A_C). i_T is continuously measured as function of V_B, which is linearly scanned from +1.5 to −1.5 V at a rate of 10 mV s^{-1}. As a consequence of the tip remaining in continuous motion, the i_T-V_B trace is recorded over regions of different conductivity, resulting in a square wave response, Figure 3B. The rectifying shape of the lower portion of the i_T-V_B response indicates that the less conductive region of the surface possesses semiconductor character. The current response in the upper portion of the trace, which is linear and indicative of ohmic behavior, is limited by the 1 MΩ value of the series resistor rather than the absolute conductance of the Ti/TiO_2 surface.

Images A and A_C of Figure 4 show deflection-mode and conductivity images of an identical region of a different Ti/TiO_2 sample, obtained at a bias voltage of +200 mV employing a 1 MΩ current-limiting resistor. As before, the C-AFM image demonstrates that the electrical conductivity of the native oxide film is heterogeneous, with ~10 000 nm^2 patches of oxide having significantly higher conductivity than the surrounding region. C-AFM images of the same region obtained at even higher resolution, e.g., image B_C (corresponding to the square area highlighted in images A and A_C), demonstrate that there is considerable variation in conductivity within these patches. Fluctuations in the conductivity that occur over length scales as small as ~10 nm are readily apparent in the higher magnification image. The i_T-V_B spectroscopy traces obtained as described above for Figure 3, and corresponding to the dashed lines marked in the high-resolution C-AFM image (Figure 4C), are presented below. Inspection of the two i_T-V_B curves reveals that the higher conductive region (line *ii*) has an ohmic response,

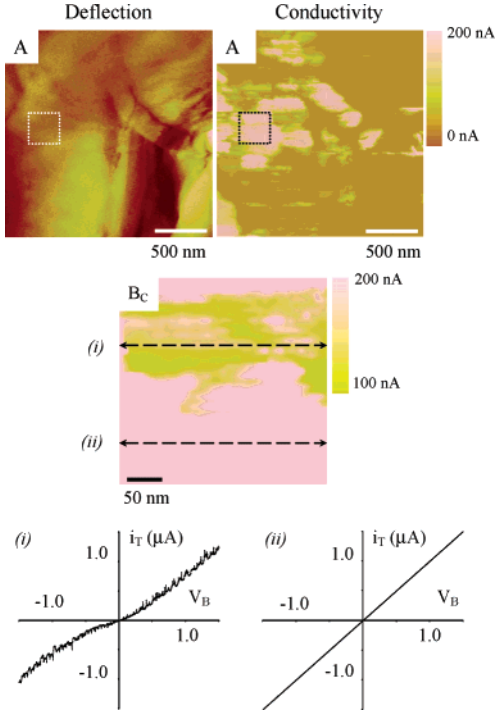

Figure 4. (A) Deflection-mode and (A_C) conductivity images of a Ti/TiO_2 surface. (B_C) High-resolution conductivity image of the region outlined by the box in image A. i_T-V_B traces obtained while continuously scanning the C-AFM tip at 10 nm s^{-1} along the dashed lines (*i*) and (*ii*). The slope of the linear i_T-V_B curve in (*ii*) is equal to the inverse value of the current-limiting resistor (1 MΩ).

limited by the current-limiting resistor, whereas the i_T-V_B curve in the less conductive region (line *i*) displays characteristics intermediate between pure ohmic and semiconductor behavior.

The conductivity of the native oxide film, σ_{oxide}, within surface regions in which the current is not limited by the instrument series resistance was estimated from the i_T-V_B curves using the relationship

$$\sigma_{oxide} = d/(A_t R_{oxide}) \quad (1)$$

where d is the oxide layer thickness (~3 nm) and A_t is the area of the C-AFM probe in contact with the surface. A_t was computed as πr_t^2, assuming a contact radius between tip and substrate of 50 nm (this value is highly approximate but the error in r_t has little effect on the qualitative conclusions presented below). R_{oxide} was estimated from the inverse slope of the i_T-V_B curve ($slope^{-1} = R_{oxide} + 1$ MΩ) evaluated at $V_B = 0$. Using this approximate approach, the conductivities of the less conductive regions in Figures 3 and 4 were estimated to be in the range 10^{-5} to 10^{-3} Ω^{-1} cm^{-1}. Thus, the more conductive regions of oxide, observed above grain boundaries and within small islands of oxide on grain faces, have a *minimum* conductivity between 10^{-3} and 10^{-1} Ω^{-1} cm^{-1}. Though this range of conductivity is still well below that of metallic Ti (2.3×10^4 Ω^{-1} cm^{-1}),[29] the magnitude of this range of values is quite large even for a moderately doped 3.05 eV band-gap semiconductor, again suggesting that the conductive regions are highly disordered or all together a different and significantly more conductive oxide phase, e.g., Ti_2O_3.

Conclusions

Ex situ C-AFM has been used to visualize the heterogeneous electronic conductivity of the ~3 nm thick native oxide film on polycrystalline Ti electrodes. C-AFM images of Ti/TiO_2 electrodes recorded in air demonstrate that the electronic conductivity of the oxide film in contact with the underlying Ti grain boundaries is at least 200× higher than the conductivity of the oxide film on grain faces. We speculate that the oxide layer is highly nonstoichiometric and defective above the grain boundaries, a consequence of the structural mismatch between intersecting oxide layers growing with different orientations and at different rates on neighboring metal grains. Large spatial variations in the oxide film conductivity on topographically featureless regions of grain faces have been tentatively attributed to the presence of nanoscale crystallites of a lower valence oxide.

Acknowledgment. Financial assistance for this research was provided by the Department of Energy Center for Excellence for the Synthesis and Processing of Advanced Materials, the *Science of Localized Corrosion*, sponsored by the Division of Materials Sciences, Office of Sciences (H.S.W.), the Royal Society University Research Fellowship (J.V.M.), and the EPSRC/RSC (C.E.G.).

References and Notes

(1) Ohtsuka, T.; Masuda, M.; Sato, N. *J. Electrochem. Soc.* **1985**, *132*, 787.
(2) Lausmaa, J.; Kasemo, B.; Mattsson, H. *Appl. Surf. Sci.* **1990**, *44*, 133.
(3) Domony, A.; Lichtenberger, E. *Metalloberflache* **1961**, *15*, 134.
(4) Tajima, S. In *Advances in Corrosion Science and Technology*; Fontana, M. G., Staehle, R. W., Eds.; Plenum Press: New York, 1970; Vol. 1.
(5) Basame, S. B.; White, H. S. *J. Phys. Chem.* **1995**, *99*, 16430.
(6) Basame, S. B.; White, H. S. *J. Phys. Chem. B* **1998**, *102*, 9812.
(7) Basame, S. B.; White, H. S. *J. Electrochem. Soc.* **2000**, *147*, 1376.
(8) Casillas, N.; Charlebois, S. J.; Smyrl, W. H.; White, H. S. *J. Electrochem. Soc.* **1993**, *140*, L144.
(9) Casillas, N.; Charlebois, S. J.; Smyrl, W. H.; White, H. S. *J. Electrochem. Soc.* **1994**, *141*, 636.
(10) Miki, T.; Yanagi, H. *Langmuir* **1998**, *14*, 3405.
(11) Jiang, F. Z.; Zhang, D. S.; Lin, Y.; Song, Y. L.; Xiao, X. R.; Jiang, L.; Zhu, D. B. *Surf. Interface Anal.* **2001**, *32*, 125.
(12) Macpherson, J. V.; Gueneau de Mussy, J. P.; Delplancke, J. L. *Electrochem. Solid State Lett.* **2001**, *4*, E33.
(13) Cronemeyer, D. C. *Phys. Rev.* **1952**, *87*, 876.
(14) Michaelis, A.; Schultze, J. W. *Thin Solid Films* **1993**, *233*, 86.
(15) Schultze, J. W.; Pilaski, M.; Lohrengel, M. M.; Konig, U. *Faraday Discuss.* **2002**, *121*, 211.
(16) Putman, C. A.; Van der Werf, K. O.; de Grooth, B. G.; van Hulst, N. F.; Greve, J. *Proc. SPIE* **1992**, *198*, 1639.
(17) Casillas, N.; Snyder, S. R.; White, H. S. *J. Electrochem. Soc.* **1991**, *138*, 641−642.
(18) Olbrich, A.; Ebersberger, B.; Boit, C.; Vancea, J.; Hoffman, H.; Altmann, H.; Gieres, G.; Wecker, J. *Appl. Phys. Lett.* **2001**, *78*, 2934.
(19) Luo, E. Z.; Wong, S. K.; Pakhomov, A. B.; Xu, J. B.; Wilson, I. H.; Wong, C. Y. *J. Appl. Phys.* **2001**, *90*, 5202.
(20) Casillas, N. Ph.D. Thesis, University of Minnesota, Minneapolis, MN, 1993.
(21) Macpherson, J. V.; Unwin, P. R. *Anal. Chem.* **2001**, *73*, 550.
(22) Ikeda, H.; Kurumado, N.; Ohmori, K.; Sakashita, M.; Sakai, A.; Zaima, S.; Yasuda, Y. *Surf. Sci.* **2001**, *493*, 653.
(23) O'Shea, S. J.; Atta, R. M.; Murrell, M. P.; Welland, M. E. *J. Vac. Sci. Technol. B* **1995**, *13*, 1945.
(24) Henrich, V. E.; Dresselhaus, G.; Zeigeer, H. J. *Phys. Rev. Lett.* **1976**, *36*, 1335−1339.
(25) Kofstad, P. *Nonstoichiometry, Diffusion, and Electrical Conductivity in Binary Metal Oxides*; Wiley-Interscience: New York, 1972.
(26) Pennycook, S. J.; Kim, M.; Duscher, G.; Browning, N. D.; Sohlberg, K.; Pantelides, S. T. In *Structure−Property Relationships of Oxide Surfaces and Interfaces*; Carter, C. B., Pan, X., Sickafus, K., Tuller, H. L., Wood, T. E., Eds.; Materials Research Society: Boston, 2000; Vol. 654, p AA1.3.
(27) Henrich, V. E.; Cox, P. A. *The Surface Science of Metal Oxides*; Cambridge University Press: Cambridge, U.K., 1994.
(28) Armstrong, N. R.; Quinn, R. K. *Surf. Sci.* **1977**, *67*, 451−468.
(29) Kittel, C. *Introduction to Solid State Physics*; Wiley: New York, 1976.